View metadata, citation and similar papers at core.ac.uk

brought to you by CORE

provided by Elsevier - Publisher Connector

International Journal of Solids and Structures 46 (2009) 1727–1735

Contents lists available at ScienceDirect

International Journal of Solids and Structures

journal homepage: www.elsevier.com/locate/ijsolstr

On the Mullins effect and hysteresis of fibered biological materials: A comparison between continuous and discontinuous damage models

Estefanía Peña [a,b,*], Juan A. Peña [c], Manuel Doblaré [a,b]

[a] Group of Structural Mechanics and Materials Modelling, Aragón Institute of Engineering Research (I3A), University of Zaragoza, María de Luna, 3, E-50018 Zaragoza, Spain
[b] Centro de Investigación Biomédica en Red en Bioingeniería, Biomateriales y Nanomedicina (CIBER-BBN), Spain
[c] Department of Management and Manufacturing Engineering, Faculty of Engineering, University of Zaragoza, Spain

ARTICLE INFO

Article history:
Received 12 November 2008
Received in revised form 9 December 2008
Available online 1 January 2009

Keywords:
Hyperelasticity
Constitutive modelling
Damage mechanics
Mullins type behavior
Biomechanics
Soft tissues

ABSTRACT

Deformation induced softening is an inelastic phenomenon frequently accompanying mechanical behavior of soft biological tissues. This paper presents and compare continuous and discontinuous damage approaches to model softening effects in fibered materials such as soft biological tissues. The structural model is formulated using the concept of internal variables that provides a very general description of materials involving irreversible effects. We consider the internal variables associated to damage to correspond to separated contributions of the matrix and the fibers. Local damage accumulation is related to two phenomenological variables, the maximum value and the arclength of the effective free energy attained during the loading process, respectively. A local multiplicative decomposition of the deformation gradient into volume-preserving and dilatational parts is used that permits to model the incompressibility property of most types of soft biological tissues. In this context, damage is related only to the isochoric part of the deformation. Finally, simulations of biaxial and uniaxial tests in two directions are used to compare the performance of both models. Numerical simulations indicate that only a mixed model that consider both, continuous and discontinuous, damage models is able to capture the softening phenomenon of soft biological tissues.

© 2008 Elsevier Ltd. All rights reserved.

1. Introduction

Constitutive modelling of soft biological tissues has been an area of extensive research in the last few years (Fung, 1993; Holzapfel, 2001; Humphrey, 2002). Accurate mechanical models of soft tissue coupled with appropriate numerical approaches can potentially aid in areas such as tissue engineering, in particular in the study of cardiovascular or orthopaedic dysfunctions, and the simulation of surgical interventions or accident trauma. When modelling the mechanical behavior of soft tissue, particular difficulties arise. Biological soft tissues are subjected to large deformations with negligible volume changes and show an anisotropic mechanical response due to their internal structure.

The purely elastic response of soft tissues is often modelled within the framework of hyperelasticity by means of the definition of a strain energy function expressed in terms of kinematic invariants, first developed by Spencer (1954). This approach was further tuned and applied to finite element simulations of soft collagenous biological tissues (see, for example, Weiss et al. (1996), Peña et al. (2007) for ligaments, Holzapfel et al. (2000) for arteries and Lanchares et al. (2008) for cornea). Even though different strain energy density functions have proved to be successful for particular applications and for describing many of the mechanical properties of the soft tissue, their use is limited, in most cases, to the range of physiological loads (Martins et al., 1998).

However, there are three important softening phenomena associated to biological tissues. First, the dependence of the mechanical response on the previously attained maximum load level very similar to the well-known Mullins effect in rubber materials (Mullins, 1947). The Mullins effect is characterized by the following features: when a virgin material sample is stretched from the undeformed state to a certain deformation, the stress–stretch curve follows the so called primary loading curve. The subsequent unloading is characterized by a softened behavior. Subsequent reloading follows the former unloading curve until the previous maximum stretch is reached. At this position the loading path swings up and traces the primary curve again up to a new maximum. Other typical phenomenon named as preconditioning is characterized by continuous softening during the early cycles until achieving a certain "saturated" state (Humphrey, 2002). The area enclosed by the loading and unloading curves, which reflects the dissipated energy, decreases with every cycle. Finally, in the steady

* Corresponding author. Address: Group of Structural Mechanics and Materials Modelling, Aragón Institute of Engineering Research (I3A), University of Zaragoza, María de Luna, 3, E-50018 Zaragoza, Spain. Tel.: +34 976761912; fax: +34 976762578.
E-mail address: fany@unizar.es (E. Peña).

0020-7683/$ - see front matter © 2008 Elsevier Ltd. All rights reserved.
doi:10.1016/j.ijsolstr.2008.12.015

state, the loading and unloading paths almost coincide. Finally, the softening as a result of the bond rupture and complete damage has to be mentioned (Volokh, 2007a).

Only a few constitutive models are able to describe the inelastic behavior of soft tissues. Hurschler et al. (1997) and Liao and Belkoff (1999) have proposed two different formulations to describe damage in soft tissue; however, these models have been restricted to the damage of the collagenous component. A pseudo-elastic model early developed by Ogden and Roxburgh (1999) to model the Mullins effect in particle-filled rubber was suggested to capture the hysteretic behavior of brain tissue by Franceschini et al. (2006). Natali et al. (2005) presented a transversely isotropic constitutive model for tendons that included elasto-damage. Hokanson and Yazdami (1997) included isotropic damage in a constitutive model for arteries. Balzani et al. (2006) assumed that discontinuous damage occurs in arterial walls and mainly along the fiber direction. Thus, they provided scalar damage variables for the transversely isotropic part of a polyconvex strain energy function. Rodríguez et al. (2006, 2008) introduced a stochastic-structurally based damage model for fibrous soft tissues. Calvo et al. (2007) proposed an uncoupled directional damage model for fibered biological soft tissues that considers different damage evolutions for the matrix and for the different fiber families. A comparison between these two models has recently been carried out by Alastrué et al. (2007). Modelling the softening as a result of the bond rupture and complete damage is usually accomplished by using the Continuum Damage Mechanics (CDM) theory, although does not necessarily, much simpler approaches can be used as recently proposed by Volokh (2007b). Finally, Ehret and Itskov (2008) presented a model where anisotropic softening is considered by means of monitoring the evolution of internal variables governing the anisotropic properties of the material.

In the present work, continuous and discontinuous damage models for biological tissues are presented and compared to model softening effects in soft biological tissues such as preconditioning and Mullins type behavior. The paper is organized as follows. Section 2 gives a brief review of the constitutive equations for anisotropic hyperelastic materials. Section 3 describes the continuous and discontinuous damage models for biological soft tissues, whereas in Section 4 the weak form of the equilibrium equations and the associated linearization are presented. In Section 5, typical evolution equations for the damage variables proposed in the literature are summarized. Section 6 shows some numerical examples of the application of both damage models previously described. Finally, Section 7 closes with some concluding remarks.

2. Constitutive modelling of hyperelastic fibrous materials

Fibrous soft tissues such as ligaments and tendons, skin, arteries, and veins are materials composed primarily of connective tissue proteins, elastin and collagen, and smooth muscle cells. Stiff collagen fibers with a given orientation are the main responsible of the tissue anisotropy. So, these materials are modelled as a matrix material and several families of fibers. In addition, soft biological tissues are subjected to large deformations with negligible volume changes, that is, only quasi-isochoric ($J \approx 1$) motions are possible.

Let $\mathbf{x} = \boldsymbol{\chi}(\mathbf{X}, t) : \Omega_0 \times \mathbb{R} \rightarrow \mathbb{R}^3$ denote the motion mapping and let $\mathbf{F}$ be the associated deformation gradient. Here, $\mathbf{X}$ and $\mathbf{x}$ define the respective positions of a particle in the reference Ω_0 and current Ω configurations such as $\mathbf{F} = \frac{d\mathbf{x}}{d\mathbf{X}}$. Further, let $J \equiv det\mathbf{F}$ be the jacobian of the motion. To properly define volumetric and deviatoric responses in the nonlinear range, we introduce the following kinematic decomposition (Flory, 1961):

$$\mathbf{F} = J^{\frac{1}{3}}\overline{\mathbf{F}}, \quad \overline{\mathbf{F}} = J^{-\frac{1}{3}}\mathbf{F} \tag{1}$$

$$\mathbf{C} = \mathbf{F}^T\mathbf{F}, \quad \overline{\mathbf{C}} = J^{-\frac{2}{3}}\mathbf{C} = \overline{\mathbf{F}}^T\overline{\mathbf{F}} \tag{2}$$

The term $J^{\frac{1}{3}}\mathbf{I}$ is associated with volume-changing deformations, while $\overline{\mathbf{F}}$ is associated with volume-preserving deformations. We shall call $\overline{\mathbf{F}}$ and $\overline{\mathbf{C}}$ the modified deformation gradient and the modified right Cauchy–Green tensors, respectively.

A frequently used strategy to incorporate anisotropy in continuum models is based on the explicit consideration of vectors, defined in the reference configuration, characterizing each direction of anisotropy at each material point (Spencer, 1954). For materials with two directions of anisotropy, it is necessary to introduce two unit vectors $\mathbf{m}$ and $\mathbf{n}$ describing the anisotropy directions, and the concept of pseudo-invariants, that are used to define the strain energy function. The following invariants and pseudo-invariants are defined

$$\begin{aligned}
&\bar{I}_1 \doteq \mathrm{tr}[\overline{\mathbf{C}}] \quad \bar{I}_2 \doteq \frac{1}{2}[[tr(\overline{\mathbf{C}})^2 - tr\overline{\mathbf{C}}^2)] \\
&\bar{I}_4 \doteq \mathbf{m}\cdot\overline{\mathbf{C}}\cdot\mathbf{m} = \overline{\mathbf{C}} : \mathbf{M} \quad \bar{I}_5 \doteq \mathbf{m}\cdot\overline{\mathbf{C}}^2\cdot\mathbf{m} = \overline{\mathbf{C}}^2 : \mathbf{M} \\
&\bar{I}_6 \doteq \mathbf{n}\cdot\overline{\mathbf{C}}\cdot\mathbf{n} = \overline{\mathbf{C}} : \mathbf{N} \quad \bar{I}_7 \doteq \mathbf{n}\cdot\overline{\mathbf{C}}^2\mathbf{n} = \overline{\mathbf{C}}^2 : \mathbf{N} \\
&\bar{I}_8 \doteq [\mathbf{m}\cdot\mathbf{n}]\mathbf{m}\cdot\overline{\mathbf{C}}\cdot\mathbf{n} \quad \bar{I}_9 \doteq [\mathbf{m}\cdot\mathbf{n}]^2
\end{aligned} \tag{3}$$

with $\bar{I}_1$ and $\bar{I}_2$ the first two strain invariants of the symmetric modified Cauchy–Green tensor $\overline{\mathbf{C}}$ (Note that $I_3 = J^2$ and $\bar{I}_3 = 1$ for incompressible materials here considered), and $\mathbf{M} = \mathbf{m}\otimes\mathbf{m}$ and $\mathbf{N} = \mathbf{n}\otimes\mathbf{n}$ are structural tensors. While the pseudo-invariants $\bar{I}_4$ and $\bar{I}_6$ have a clear physical meaning, the square of the stretch $\lambda_{(m,n)}$ in the fibers directions, the influence of the rest of pseudo-invariants $\bar{I}_5$, $\bar{I}_7$, and $\bar{I}_8$ is difficult to evaluate due to the high correlation between them. For this reason and the lack of sufficient experimental data, it is usual not to include these invariants in the definition of the strain energy function Ψ (Spencer, 1954). Finally, the pseudo-invariant $\bar{I}_9$ does not depend on the deformation, so it does not have any relations with the strain energy.

The associated strain energy function for anisotropic materials is therefore written as

$$\Psi = \Psi_{\mathrm{vol}}(J) + \Psi_{\mathrm{ich}}(\overline{\mathbf{C}}, \mathbf{M}, \mathbf{N}) = \Psi_{\mathrm{vol}}(J) + \Psi_{\mathrm{ich}}(\bar{I}_1, \bar{I}_2, \bar{I}_4, \bar{I}_6) \tag{4}$$

The second Piola–Kirchhoff stress tensor is obtained by derivation of (4) with respect to the right Cauchy–Green tensor. Thus, the stress tensor consists of a purely volumetric and a purely isochoric contribution, i.e. $\mathbf{S}_{\mathrm{vol}}$ and $\mathbf{S}_{\mathrm{ich}}$, so the total stress is

$$\mathbf{S} = \mathbf{S}_{\mathrm{vol}} + \mathbf{S}_{\mathrm{ich}} = 2\frac{\partial\Psi_{\mathrm{vol}}}{\partial\mathbf{C}} + 2\frac{\partial\Psi_{\mathrm{ich}}}{\partial\mathbf{C}} = Jp\mathbf{C}^{-1} + 2\sum_{j=1,2,4,6}\frac{\partial\Psi_{\mathrm{ich}}}{\partial\bar{I}_j}\frac{\partial\bar{I}_j}{\partial\overline{\mathbf{C}}} : \frac{\partial\overline{\mathbf{C}}}{\partial\mathbf{C}} \tag{5}$$

Note that it is possible to obtain the Cauchy stress tensor by applying the push-forward operation to (5) (Holzapfel, 2000).

Based on the kinematic decomposition of the deformation gradient tensor, the tangent operator, also known as elasticity tensor when dealing with elastic constitutive laws, is defined in the reference configuration as

$$\mathbf{C} = 2\frac{\partial\mathbf{S}(\mathbf{C}, \mathbf{M})}{\partial\mathbf{C}} = \mathbf{C}_{\mathrm{vol}} + \mathbf{C}_{\mathrm{ich}} = \mathbf{C}_{\mathrm{vol}} + 4\frac{\partial^2\Psi_{\mathrm{ich}}(\bar{I}_1, \bar{I}_2, \bar{I}_4, \bar{I}_6)}{\partial\mathbf{C}^2} \tag{6}$$

Note that the spatial counterpart is obtained from the application of the push-forward operation to (6).

3. Continuous and discontinuous damage models for fibered materials

In Continuum Damage Mechanics, the free energy for the fibers is assumed to be of the form (Souza-Neto et al., 1998)

$$\Psi(\mathbf{C},\mathbf{M},\mathbf{N},D_k) = \Psi^0_{\text{vol}}(J) + \sum_{k=m,f_1,f_2} \Psi_{\text{ich}(k)} = \Psi^0_{\text{vol}}(J) + \sum_{k=m,f_1,f_2} [1-D_k]\Psi^0_{\text{ich}(k)} \tag{7}$$

where $(1-D_k)$ are known as the reduction factors (Simo, 1987), being the internal variables $D_k \in [0,1]$ normalized scalars referred to as the damage variables, for the matrix, D_m, and the two families of fibers, D_{f4} and D_{f6}, respectively (Calvo et al., 2007).

Using standard arguments based on the Clausius–Duhem inequality (Marsden and Hughes, 1994)

$$\mathscr{D}_{int} = -\dot{\Psi} + \frac{1}{2}\mathbf{S}:\dot{\mathbf{C}} \geqslant 0 \tag{8}$$

and Eqs. (7) to (8) gives (Calvo et al., 2007):

$$\mathscr{D}_{int} = \left[\mathbf{S} - J\frac{d\Psi^0_{\text{vol}}(J)}{dJ}\mathbf{C}^{-1} - 2J^{\frac{-2}{3}}\sum_{k=m,f_1,f_2}\mathbf{P}:[1-D_k]\frac{\partial\Psi^0_{\text{ich}(k)}}{\partial\overline{\mathbf{C}}}\right]:\frac{\dot{\overline{\mathbf{C}}}}{2} + \sum_{k=m,f_1,f_2}\frac{\partial\Psi_{\text{ich}(k)}}{\partial D_k}\dot{D}_k \geqslant 0 \tag{9}$$

where the fourth-order tensor $\mathbf{P} = \mathbf{I} - \frac{1}{3}\mathbf{C}^{-1}\otimes\mathbf{C}^{-1}$ is the projection tensor with respect to the reference configuration (Holzapfel, 2000) with $\Psi^0_{\text{ich}(k)}(k = m,f_1,f_2)$ being the contributions of the matrix and the two families of fibers, respectively. Eq. (9) leads to the representation

$$\mathbf{S} = 2\frac{\partial\Psi(\mathbf{C},\mathbf{M})}{\partial\mathbf{C}} = \mathbf{S}_{\text{vol}} + \sum_{k=m,f_1,f_2}[1-D_k]\mathbf{S}^0_{\text{ich}} \tag{10}$$

where $\mathbf{S}_{\text{vol}}$ and $\mathbf{S}^0_{\text{ich}}$ denote a purely volumetric and a purely isochoric effective contribution of the stress tensor of the undamaged material (5), whereas the principle of positive dissipation leads to

$$\mathscr{D}_{int} = \sum_{k=m,f_1,f_2} f_k\dot{D}_k \geqslant 0 \tag{11}$$

with f_k conjugate state functions of the internal variables D_k defined as

$$\begin{aligned} f_m &= -\frac{\partial\Psi_{\text{ich}(m)}}{\partial D_m} = \Psi^0_{\text{ich}(m)}(\overline{\mathbf{C}}) \geqslant 0 \\ f_{f_1} &= -\frac{\partial\Psi_{\text{ich}(f1)}}{\partial D_{f_1}} = \Psi^0_{\text{ich}(f1)}(\overline{\mathbf{C}},\mathbf{M}) \geqslant 0 \\ f_{f_2} &= -\frac{\partial\Psi_{\text{ich}(f2)}}{\partial D_{f_2}} = \Psi^0_{\text{ich}(f2)}(\overline{\mathbf{C}},\mathbf{N}) \geqslant 0 \end{aligned} \tag{12}$$

In order to complete the constitutive model we have to determine the evolution equation for the internal damage variables D_k. First, a Mullins-type discontinuous damage evolution is assumed where the damage accumulation occurs only within the first cycle of a strain-controlled loading process. Further strain cycles below the maximum effective strain energy reached will not contribute to this type of damage. Second, we take into account independently of the mechanism above, a continuous damage accumulation within the whole strain history of the deformation process which is also governed by the local effective strain energy (Miehe and Keck, 2000). The total damage is then described by the constitutive expression

$$D_k \doteq D^\alpha_k(\alpha) + D^\beta_k(\beta) \tag{13}$$

where $D^\alpha_k:\mathbb{R}_+\to\mathbb{R}_+$ and $D^\beta_k:\mathbb{R}_+\to\mathbb{R}_+$ are monotonically increasing smooth functions with the following properties $D^\alpha_k(0)=0, D^\beta_k(0)=0$ and $D^\alpha_k(\alpha)+D^\beta_k(\beta)\in[0,1]\ \forall\alpha,\beta$. They can be considered as shape functions which relate the damage variables D_k to the new variables α and β which describe the discontinuous and the continuous damage, respectively. These new variables are related to the evolution of the damage driving forces f_k as follows.

The *discontinuous damage* (Mullins-type) is assumed to be governed by the variable

$$\alpha_k(t) \doteq \max_{s\in(-\infty,t)}\sqrt{2\Psi^0_{\text{ich}(k)}(\overline{\mathbf{C}}(s))} \tag{14}$$

Thus, $\alpha(t)$ is simply the maximum thermodynamic force or effective strain energy which has been achieved within the loading history interval $[0,t)$. We define a damage criterion in the strain space by the condition that, at any time t of the loading process, the following expression is fulfilled (Simo, 1987)

$$\Phi_k(\overline{\mathbf{C}}(t),\Xi_{k_t}) = \sqrt{2\Psi^0_{\text{ich}(k)}(\overline{\mathbf{C}}(t))} - \alpha_k(t) = \Xi_k - \alpha_k(t) \leqslant 0 \tag{15}$$

The equation $\Phi_k(\overline{\mathbf{C}}(t),\Xi_{k_t}) = 0$ defines a damage surface in the strain space. Finally, the evolution of the damage parameters D_k is characterized by an irreversible equation of evolution such as (Calvo et al., 2007)

$$\frac{dD^\alpha_k}{dt} = \begin{cases} \bar{h}_k(\Xi_k,\alpha_k)\dot{\Xi}_k & \text{if} \quad \Phi_k = 0 \quad \text{and} \quad \mathbf{N}_k:\dot{\mathbf{C}} > 0 \\ 0 & \text{otherwise} \end{cases} \tag{16}$$

This underlines the discontinuous character of this damage effect. There is no damage accumulation if the thermodynamic force f_k lies inside an undamaged domain $\mathbb{D}_\alpha := \{\Xi_k\in\mathbb{R}_+ | \Xi_k - \alpha_k(t)\leqslant 0\}$. Here, $\mathbf{N}_k := \frac{\partial\phi_k}{\partial\overline{\mathbf{C}}}$ is the normal to the damage surface in the strain space, Ξ_k are defined at the current time s and $\bar{h}_k(\Xi_k,\alpha_k)$ are given functions that characterize the damage evolution in the material.

Continuous damage is assumed to be governed by the arclength of the respective driving damage force or effective strain energy.

$$\beta_k(t) \doteq \int_0^t |\dot{f}_k(s)|ds \tag{17}$$

Thus, we have the simple evolution equation

$$\dot{\beta}_k = |\dot{f}_k| = \text{sign}(\dot{\Psi}^0_{\text{ich}(k)})$$

with the initial condition $\beta_k(0)=0$. Therefore β_k monotically increase within the deformation process.

The iterative Newton procedure to solve a nonlinear finite element problem requires the determination of the consistent tangent material operator. This can be derived analytically for the given material Eq. (6). The symmetric algorithmic material tensor is expressed as (Simo, 1987)

$$\mathbf{C} = \mathbf{C}^0_{\text{vol}} + \sum_{k=m,f_1,f_2}\left[[1-D_k]\mathbf{C}^0_{\text{ich}(k)} - \bar{g}'_{(k)}\mathbf{S}^0_{\text{ich}(k)}\otimes\mathbf{S}^0_{\text{ich}(k)}\right] \tag{18}$$

with the continuous tangent factor $\bar{g}'_{(k)}$ defined as

$$\bar{g}'_{(k)} = \begin{cases} \dot{D}^\alpha_k(\alpha) + \dot{D}^\beta_k(\beta)\text{sign}(\dot{f}_k) & \text{if} \quad \Phi_k = 0 \quad \text{and} \quad \mathbf{N}_k:\dot{\mathbf{C}} > 0 \\ \dot{D}^\beta_k(\beta)\text{sign}(\dot{f}_k) & \text{otherwise} \end{cases} \tag{19}$$

This completes the constitutive formulation of anisotropic finite strain elasticity with damage-caused energy-based softening effects. This results in a symmetric algorithmic tangent modulus, essential for the solution of the implicit finite element equations.

4. Evolution equations for the internal damage variables

Typical evolution equations for the discontinuous damage variables, D^α_k, proposed in the literature for fibered materials such as soft biological tissues have been used. They correspond to the following expressions (Calvo et al., 2007; Peña et al., 2008a; Rodríguez et al., 2008)

$$D_k^{\alpha}(\Xi_{k_t}) \doteq \begin{cases} 0 & \text{if} \quad \Xi_{k_t} < \Xi^0_{min_k} \\ 1-\dfrac{1-\exp(\mu_k[\Xi^k_t - \Xi_{max_k}])}{1-\exp(\mu_k[\Xi_{min_k} - \Xi_{max_k}])} & \text{if} \quad \Xi^0_{min_k} \leqslant \Xi_{k_t} \leqslant \Xi^0_{max_k} \\ 1 & \text{if} \quad \Xi_{k_t} > \Xi^0_{max_k} \end{cases} \tag{20}$$

$$D_k^{\alpha}(\Xi_{k_t}) \doteq \begin{cases} 0 & \text{if} \quad \Xi_{k_t} < \Xi^0_{min_k} \\ \Lambda_k^2[1-\eta_k[\Lambda_k^2-1]] & \text{if} \quad \Xi^0_{min_k} \leqslant \Xi_{k_t} \leqslant \Xi^0_{max_k} \\ 1 & \text{if} \quad \Xi_{k_t} > \Xi^0_{max_k} \end{cases} \tag{21}$$

$$D_k^{\alpha}(\Xi_{k_t}) \doteq \frac{1}{2}\left[1+\frac{2\xi_k\Xi_{k_t}\exp(2\xi_k[[2\Xi_{k_t}/\rho_k]-1])-1}{2\xi_k\Xi_{k_t}\exp(2\xi_k[[2\Xi_{k_t}/\rho_k]-1])+1}\right] \tag{22}$$

with $0 \leqslant \Lambda = \frac{\Xi_{k_t}-\Xi^0_{min_k}}{\Xi^0_{max_k}-\Xi^0_{min_k}} \leqslant 1$ a dimensionless variable and $\Xi^0_{min_k}$ the variables (14) associated to the strain energies at initial damage for matrix and fibers, respectively, $\Xi^0_{max_k}$ the variables (14) associated to the strain energy at total damage for matrix and fibers, and $\eta_k \in [-1.0, 1.0]$, $\mu_k \geqslant 0$, $\xi_k \geqslant 0$ and $\rho_k \geqslant 0$ are model parameters.

Some remarks are needed regarding the previous evolution equations for the discontinuous damage variables, D_k^{α}. When $\Xi_{k_t} = \Xi^0_{max_k}$, Eq. (20) has not first continuous derivative, so some numerical problems could appear. Eq. (21) is a non-monotonically increasing function for the material parameter η_k outside the interval $[-1.0, 1.0]$. This implies that the quality of the fitting of experimental data may be low when constants are restricted by stability considerations. In addition, in Eq. (22), we can not control damage initiation since the parameters $\Xi^0_{min_k}$ and $\Xi^0_{max_k}$ are not considered. With all this in the mind, we consider the new evolution equation

$$D_k^{\alpha}(\Xi_{k_t}) \doteq \begin{cases} 0 & \text{if} \quad \Xi_{k_t} < \Xi^0_{min_k} \\ \frac{1}{2}\left[1+\dfrac{2\zeta_k\Lambda_k\exp(2\zeta_k[2\Lambda_k-1])-1}{2\zeta_k\Lambda_k\exp(2\zeta_k[2\Lambda_k/\rho_k]+1)}\right] & \text{if} \quad \Xi^0_{min_k} \leqslant \Xi_{k_t} \leqslant \Xi^0_{max_k} \\ 1 & \text{if} \quad \Xi_{k_t} > \Xi^0_{max_k} \end{cases} \tag{23}$$

that is convex for $\zeta_k \geqslant 0$ (Fig. 1).

Finally, the continuous damage D_k^{β} is assumed to have the form

$$D_k^{\beta} = d^{\beta}_{k\infty}\left[1-\exp\left(-\frac{\beta}{\gamma_k^{\beta}}\right)\right]$$

Note that the parameters $d^{\beta}_{k\infty}$ describe the maximum possible continuous damage. Thus we have the constraint $d^{\beta}_{k\infty} \in [0, 1]$. We refer to γ_k^{β} as the damage saturation parameters.

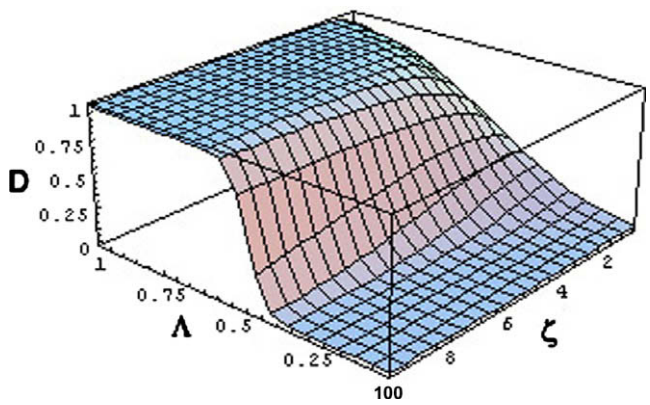

Fig. 1. Damage evolution for the modified sigmoidal function (23) with $0 \leqslant \Lambda \leqslant 1$ and $\zeta_k \geqslant 0$.

5. Weak formulation

The spatial version of the principle of virtual work is written as:

$$\delta W(\mathbf{u}, \delta\mathbf{u}) = \delta W_{int}(\mathbf{u}, \delta\mathbf{u}) + \delta W_{ext}(\mathbf{u}, \delta\mathbf{u}) \tag{24}$$

where

$$\delta W_{int}(\mathbf{u}, \delta\mathbf{u}) = \int_{\Omega} \boldsymbol{\sigma} : \delta\mathbf{e}\, dv \tag{25}$$

being $\mathbf{e} = \frac{1}{2}(\mathbf{I} - \mathbf{F}^{-T}\mathbf{F}^{-1})$ the Euler–Almansi strain tensor.

$$\delta W_{ext}(\mathbf{u}, \delta\mathbf{u}) = \int_{\Omega} \rho[\mathbf{b} - \ddot{\mathbf{u}}] \cdot \delta\mathbf{u}\, dv + \int_{\partial\Omega_{\sigma}} \bar{\mathbf{t}} \cdot \delta\mathbf{u}\, ds \tag{26}$$

and δ the appropriate linearization of each quantity in the direction of the admissible variation $\delta\mathbf{u}$, described below.

We shall consider a purely static problem, so that $\ddot{\mathbf{u}} = \mathbf{0}$. In addition, we assume that the external loads (the body forces $\mathbf{b}$ and the surface traction $\bar{\mathbf{t}}$) are 'dead' (independent of the deformation), so that the linearization of the external virtual work vanishes, i.e. $D_{\triangle\mathbf{u}}\delta W_{ext}(\mathbf{u}, \delta\mathbf{u}) = \mathbf{0}$. Hence, the linearization of the variational Eq. (24) only affects to the internal virtual work δW_{int}, which will be considered below. The idea is first to pull-back the spatial quantities to the reference configuration (internal virtual work in the material description), then to linearize and to push-forward again (Lie linearization Marsden and Hughes, 1994). Starting with the equivalent pull-back

$$\delta W_{int}(\mathbf{u}, \delta\mathbf{u}) = \int_{\Omega} \boldsymbol{\sigma}(\mathbf{u}) : \delta\mathbf{e}(\mathbf{u}) dv = \int_{\Omega_0} \mathbf{S}(\mathbf{E}(\mathbf{u})) : \delta\mathbf{E}(\mathbf{u}) dV \tag{27}$$

with $\mathbf{E} = \frac{1}{2}(\mathbf{F}^T\mathbf{F} - \mathbf{I})$ the Green–Lagrange strain tensor, we consider now the linerization of the internal virtual work in the material description

$$D_{\triangle\mathbf{u}}\delta W_{int}(\mathbf{u}, \delta\mathbf{u}) = \int_{\Omega_0} [\delta\mathbf{E}(\mathbf{u}) : D_{\triangle\mathbf{u}}\mathbf{S}(\mathbf{E}(\mathbf{u})) + \mathbf{S}(\mathbf{E}(\mathbf{u})) : D_{\triangle\mathbf{u}}\delta\mathbf{E}(\mathbf{u})] dV \tag{28}$$

The first term corresponds to the material stiffness matrix and the second to the geometric part of the stiffness matrix. We can then write

$$\begin{aligned} D_{\triangle\mathbf{u}}\delta W_{int}(\mathbf{u}, \delta\mathbf{u}) = \int_{i\Omega_0} [&\delta\mathbf{E}(\mathbf{u}) : \mathbf{C}(\mathbf{u}) : D_{\triangle\mathbf{u}}\mathbf{E}(\mathbf{u}) + \mathbf{S}(\mathbf{E}(\mathbf{u})) \\ &: D_{\triangle\mathbf{u}}\delta\mathbf{E}(\mathbf{u})] dV \end{aligned} \tag{29}$$

Considering the push-forward operations already derived, from (29) and taking into account the relation $dv = JdV$, the linearized virtual work in the spatial description may be written as (Holzapfel, 2000)

$$\begin{aligned} &D_{\triangle\mathbf{u}}\delta W_{int}((\mathbf{u}), \delta\mathbf{u}) \\ &= \int_{\Omega} \left[\frac{\partial\delta u_a}{\delta x_b}\mathbf{c}_{abcd}\frac{\partial\triangle u_c}{\delta x_d} + \frac{\partial\delta u_a}{\delta x_b}\frac{\partial\triangle u_a}{\delta x_d}\sigma_{bd}\right] dv \\ &= \int_{\Omega} \frac{\partial\delta u_a}{\delta x_b}[\mathbf{c}_{abcd} + \delta_{ac}\sigma_{bd}]\frac{\partial\triangle u_c}{\delta x_d} dv \end{aligned} \tag{30}$$

where $(\mathbf{c} + \boldsymbol{\delta} \otimes \boldsymbol{\sigma})$ represents the elasticity tensor that includes the material and geometric parts of the consistent tangent stiffness matrix.

6. Numerical examples

The continuous and discontinuous damage models here presented were implemented into the general-purpose finite element software ABAQUS (Hibbit, Karlsson., Sorensen, Inc., 2006) by means of a UMAT subroutine. The mechanical problem was solved using a fully geometrically nonlinear formulation. In order to illustrate the performance and the physical mechanisms involved in the consti-

Table 1
Material and damage parameters for biaxial simple tension. C_1, C_2, and C_3 are in MPa, Ξ is in $MPa^{1/2}$ and other parameter are dimensionless.

C_1	C_2	C_3	C_4	D					
0.056	0.0	1.37	1.095	0.00001					
Ξ^m_{min}	Ξ^m_{max}	ζ^m	$d^\beta_{m\infty}$	γ^β_m	Ξ^f_{min}	Ξ^f_{max}	ζ^f	$d^\beta_{f\infty}$	γ^β_f
0.0	2.1	0.55	0.25	2.0	0.0	6.15	0.82	0.25	3.0

tutive model presented herein, we analyzed several examples that correspond to different tissues under some typical experimental tests.

6.1. Influence of continuous and discontinuous damage: biaxial simple tension

A biaxial test on a plane strain problem is presented in this example. Some differences between continuous, discontinuous and mixed (continuous and discontinuous) damage models are shown herein. Only one family of fibers is defined along the X direction. The particular form of the deviatoric function Ψ_{ich} is defined in (31) (Natali et al., 2005) and the volumetric part of the strain energy function is always stated as $\Psi_{\text{vol}} = \frac{1}{D}\ln^2(J)$ (Holzapfel, 2000).

$$\Psi^0_{\text{ich}(m)} = C_1[\bar{I}_1 - 3] + C_2[\bar{I}_2 - 3]$$
$$\Psi^0_{\text{ich}(f1)} = \frac{C_3}{C_4}[\exp(C_4[\bar{I}_4 - 1]) - C_4[\bar{I}_4 - 1] - 1] \tag{31}$$

The specimen is subjected to cyclic stretching at the same time in both directions (X and Y) monitoring the stress response. Three cyclic test with different mean stretches $\lambda_1 = 1.35$, $\lambda_2 = 1.46$, and $\lambda_3 = 1.56$ were analyzed. The results of a mixed continuous and discontinuous damage model, a purely continuous damage model and a purely discontinuous damage model were all compared using the material parameters shown in Table 1.

The obtained results from the finite element simulation are presented in Fig. 2 as nominal stress versus stretch along the loading direction for the matrix and the fibers (σ_y and σ_x, respectively). One can observe a strong anisotropy of the material with respect to both the stress and the softening characteristics. In the purely discontinuous damage case, it is easy to detect the characteristic Mullins's damage with damage only occurring during the loading process. On the contrary, in the purely continuous damage case, damage occurs in both loading and unloading that increases faster in the initial loading history $\lambda_1 = 1.35$ than at the end $\lambda_3 = 1.56$. Finally, in the mixed damage case under loading damage strongly increases whereas during unloading damage is lower in special when becomes close to the stabilized value as shown in Fig. 3. This behavior is similar to the hysteretic effects in Mullins's damage (Mullins, 1947), so only the mixed damage model can reproduce this phenomena since the purely continuous or discontinuous models can not reproduce both effects separately.

6.2. A sensitivity analysis of the damage parameters

To gain a deeper insight into the effect of the different model parameters on the predicted material response, a sensitivity analysis has been carried out. Due to the discontinuous damage model was previously presented in Calvo et al. (2007), we only consider here the sensitivity analysis for continuous damage model parameters. The study comprises the effect of the maximum possible continuous damage, $d^\beta_{k\infty}$, and the damage saturation parameter, γ^β_k.

Fig. 4 depicts the sensitivity of the damage evolution and σ_x to changes on the maximum possible continuous damage, $d^\beta_{k\infty}$, for $\gamma^\beta_k = 3.0$. The results show that continuous damage, as well as total damage increases, as $d^\beta_{f\infty}$ increases. Also, the slope of the continuous damage curve seems to increase as $d^\beta_{f\infty}$ increases. However, the damage saturation region (stretch where saturation occurs) does not appear to change significantly. On the other hand, larger values of $d^\beta_{f\infty}$ lead to lower values of the deformation and stress at which maximum damage occurs while the maximum stress in the stress–strain curve decreases.

Fig. 5 depicts the sensitivity of the damage evolution and σ_x to changes on the damage saturation parameter, γ^β_k, for $d^\beta_{k\infty} = 0.25$. A remarkable influence of this parameter on the continuous damage is obtained. A considerable decrement of the slope of the continuous damage appears close to the value of the maximum continuous damage reached. On the other hand, lower values of γ^β_k lead to higher values of the deformation and stress at which maximum damage occurs while the maximum stress in the stress–strain curve decreases. This result is expected since γ^β_k controls the saturation and the rate increase of continuous damage.

6.3. Softening behavior of arteries

In this example, we compare the model presented here with experimental stress–stretch data from uniaxial cyclic loading tests on arterial tissue. These experiments were developed in our laboratory in order to study the properties of the pig aorta tissue. Longitudinal strips, approximately 5 mm wide and 15 mm long, were resected in the circumferential an longitudinal directions where

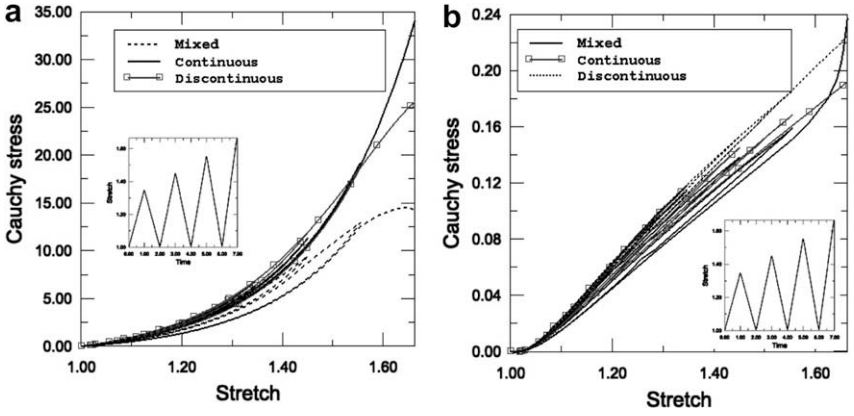

Fig. 2. Biaxial stress response under cyclic biaxial tension for the mixed, continuous and discontinuous damage models (a) σ_x and (b) σ_y.

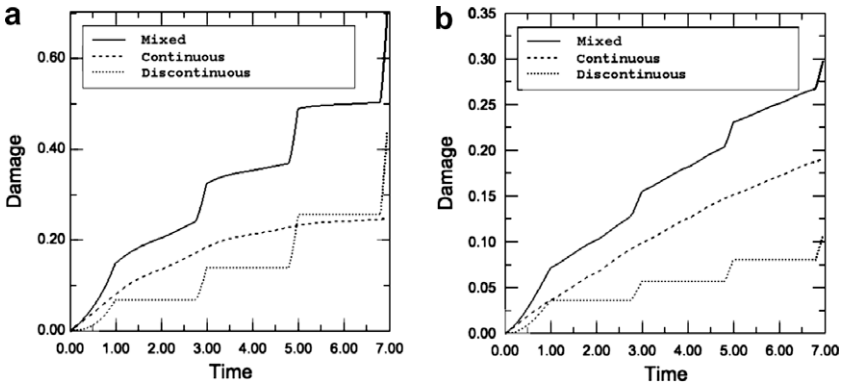

Fig. 3. Damage evolution for matrix and fibers for the mixed, continuous and discontinuous damage models.

collagen and elastic fibers are predominately oriented. Two circular black spots were painted on the surface of the strip to measure the deformation. Due to stroke limitations of the issue, "dogbone" specimens could not be used in the experiments. Instead, parallel sided (prismatic) strip specimens are used. In all experiments, the tags are placed at least 5 mm away from the grips to ensure that a uniform uniaxial region exists between them.

Different loading and unloading cycles were applied (120, 240, and 480 kPa) at 30%/min of strain rate in a high precision drive system, adapted for biological specimens (Instron Microtester 5848). Force was measured with a 50 N load cell with minimal resolution of 0.001 N. The axial stretch ratio of the specimen is measured by a non-contacting laser video-extensometer Instron 2663-281, equipped with a high performance digital camera with a megapixel sensor (0.5 ± 0.5% μm) and an IEEE 1394 (Firewire) digital interface that provides both high resolution and high data rates (50 Hz). All the tests were performed in a 100% humid atmosphere to prevent specimen drying up. Some of them, both intact and tested, were conserved after the test for histological purposes. Room temperature (~25 °C) was controlled during the experiments (Alastrué et al., 2008). The maximum load for each cycle was progressively increased and then followed by an unloading cycle with a force value close to zero. Three preliminary cycles at all load levels were applied in order to precondition the sample.

An exponential behavior to represent the collagen fibers contribution, only considered under tension, was chosen. This model, including two directions of anisotropy, was specifically designed for the arterial tissue (Holzapfel et al., 2000) and was subsequently modified in Holzapfel et al. (2005).

$$\Psi_{\text{ich}}(\overline{\mathbf{C}},\mathbf{M},\mathbf{N}) = \mu[\bar{I}_1 - 3] + \frac{k_1}{2k_2}\sum_{i=4,6}[\exp(k_2[\bar{I}_i - 1]^2) - 1] \tag{32}$$

Experimental and numerical results for loading, partial unloading and reloading are shown in Fig. 6 for the mixed, continuous and discontinuous damage models. The corresponding material parameters are summarized in Table 2. In the experimental results, in an undeformed stress-free state, i.e. at $\lambda = 1$, the slope of the uniaxial stress–stretch curve for the stress-softened material is lower than that of the virgin material and also lower than that of any previously softened material. At the unloading point, that is, when $\dot{\lambda} < 0$ and $\Phi = 0$, the slope of the uniaxial stress–stretch curve for the current stress-softened material will be greater than that of the virgin material.

The comparison between experimental tests and simulation shows a good agreement for the mixed model (see Fig. 6.a) where hysteretic and Mullins behaviors can be reproduced. However, continuous and discontinuous models are not able to reproduce the inelastic response of the aorta. The discontinuous model reproduces the Mullins effect and not the hysteretic behavior Fig. 6b, while the continuous model is able to model the hysteretic response and not the Mullins effect Fig. 6c.

Some remarks are needed regarding the mixed model in Fig. 6a. There is a very good agreement for the mixed model in the second and third cycles and not so good for the first one. The results of the simulation clearly show that the response to cyclic loading up to a certain load limit stabilizes after a several cycles (second and third cycle). Decreasing the initial damage limit however enables further softening (first cycle of the experiment). It should be noted also that the aorta, as several soft biological tissues, exhibited removal of the stress. The worse fit in the first cycle with respect the second and third ones could be explained by this phenomenon.

7. Discussion and conclusions

During the last decades a considerable growing interest has raised in modelling mechanical response of rubbery polymers.

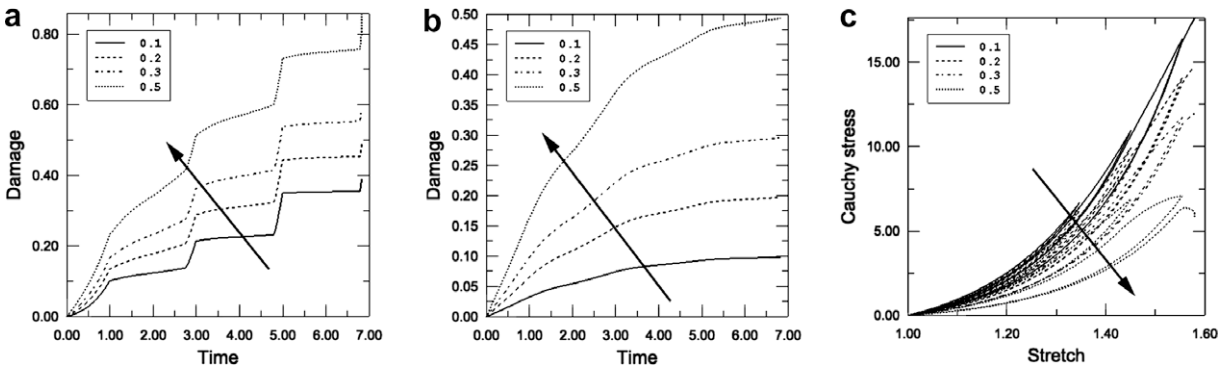

Fig. 4. Damage evolution and σ_x for different values of $d^{\beta}_{f\infty} = [0.1, 0.2, 0.3, 0.5]$ at constant $\gamma^{\beta}_{f} = 3.0$ (a) total damage; (b) continuous damage (a) σ_x.

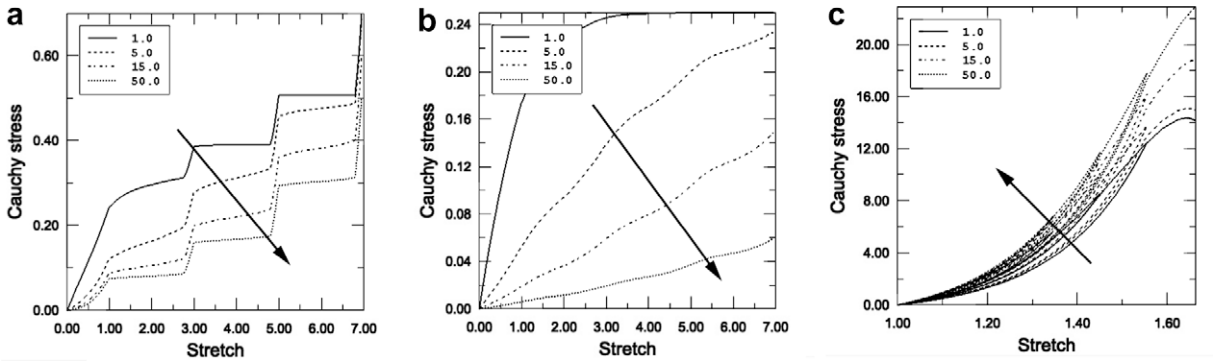

Fig. 5. Damage evolution and σ_x for different values of $\gamma_f^\beta = [1.0, 5.0, 15.0, 50.0]$ at constant $d_{f\infty}^\beta = 0.25$ (a) total damage; (b) continuous damage; (c) σ_x.

These models that initially were developed to model elastomers have been extended to model soft biological tissues in the last years. There are mainly three approach to model Mullins effect and hysteric response of materials. The first approach is based on Continuum Damage Mechanics (Simo and Ju, 1987; Govindjee and Simo, 1992; Souza-Neto et al., 1998; Kaliske et al., 2001) and has been used to model soft biological tissues (Natali et al., 2005; Calvo et al., 2007; Rodríguez et al., 2008). The second approach uses the theory of pseudo-elasticity due to Ogden and Roxburgh (1999) originally developed to model the Mullins effect and after extended to model hysteretic response (Dorfmann and Ogden, 2003) and to model permanent deformation in rubbers (Dorfmann and Ogden, 2004). Following a similar approach, Franceschini et al. (2006) used the theory of pseudo-elasticity to model the hysteretic behavior of brain tissue. And finally, the third approach is related to the hard and soft phase microstructure of vulcanized rubbers originally developed by Mullins and Tobin (1957) that was used by Qi and Boyce (2007) to model stretch-induced softening of elastomeric materials.

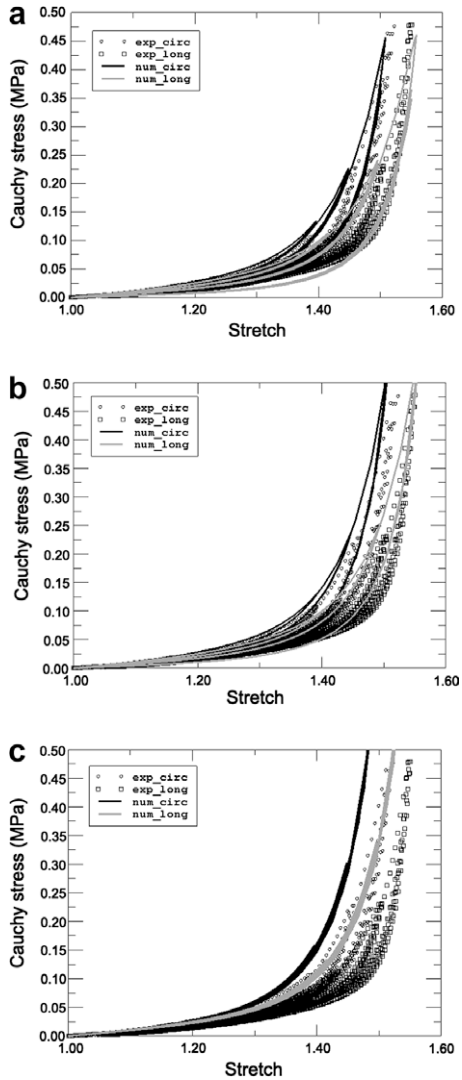

Fig. 6. Stress response under cyclic uniaxial tension for aorta tissue for the mixed, continuous and discontinuous damage models. Material and damage parameters for biaxial simple tension. μ and k_1 are in MPa, Ξ is in $\text{MPa}^{1/2}$ and other parameter are dimensionless (a) mixed model; (b) discontinuous model; (c) continuous model.

Nevertheless, all these models can not reproduce at the same time the Mullins effect and the hysteric response of soft biological tissues. For this reason, in this paper, a mixed (continuous and discontinuous) damage model, originally developed by Miehe (1995) has been extended to provide a constitutive model for quasi-static loading–unloading of soft biological tissues in order to include different softening phenomena for matrix and fibers. The model adopts the Continuum Damage Mechanics concept based on two internal variables that take into account the continuous and discontinuous evolutions, respectively. Following Miehe (1995), to model the damage process in elastomers, the local damage accumulation has been related to (i) the maximum value and (ii) the arclength of effective free energy of the past deformation history. This results in (i) a discontinuous and (ii) a continuous contribution to the damage evolution within a typical deformation-controlled cyclic loading process. To simulate the damage properties of biological soft tissues, we considered different damage evolutions for the matrix and the different families of fibers.

By means of several examples the good performance and the physical mechanisms inherent to the constitutive model presented herein have been shown. Simple tests of biological tissues have been carried out under cyclic loading conditions. These examples show that the proposed material law is able to characterize the constitutive responses of soft biological tissues effectively (preconditioning at different upper limits including hysteresis, stabilization, and Mullins' type softening). In this sense, an accurate agreement of the results of this model with the experimental data on pig aorta tissue has been achieved.

The present study has, however, some important limitations. The most remarkable is the need of a suitable experimental plan to obtain the many parameters involved (continuous and discontinuous parameters for matrix and fiber). Other limitation is that the softening behavior of biological tissues is also related to viscoelastic effects (Peña et al., 2008c). In special, in Fig. 6 the slightly

Table 2
Material and damage parameters for arterial tissue.

μ	k_1	k_2	D						
0.036147	0.000582	3.675678	0.00006						
Ξ^m_{min}	Ξ^m_{max}	ζ^m	$d^\beta_{m\infty}$	γ^β_m	Ξ^f_{min}	Ξ^f_{max}	ζ^f	$d^\beta_{f\infty}$	γ^β_f
0.08	0.41	0.61	0.45	15.0	0.01	0.465	1.06	0.507	2.55

hardened reloading behavior to the possible presence of viscoelastic effects. Continuous damage only can model hysteresis and stabilization in the first cycles of the loading path due to the fast damage saturation. The experimental data presented seem to demonstrate that the Mullins effect and hysteresis are minor tiny phenomena in cyclic loading of the pig aorta. Probably, more complex softening behavior that includes viscoelastic effects (Peña et al., 2008a) and internal structural alterations of the material (taken into account the evolution of material parameters (Ehret and Itskov, 2008) can help to complete this softening model. Finally, one numerical problem concerning the finite element implementation should be addressed (Peña et al., 2008b). It is related with the necessity to regularize the ill-posed numerical problem where the loss of ellipticity/hyperbolicity of the governing equations with softening can lead to pathological mesh-sensitivity (Bazant and Jirasek, 2002).

In spite of all these limitations, a good qualitative agreement was found between numerical and experimental results, indicating that the constitutive damage model can capture the typical stress–strain behavior observed in fibrous soft tissue. Some possible applications may be mentioned such as sports (skiing, basketball, soccer) and traffic accidents that are the most important causes of ligament injury. Vascular surgery simulations (balloon angioplasty, arterial clamping or stenting), corneal laser interventions or plastic surgery are other interesting applications to be considered in the near future.

Acknowledgement

The authors gratefully acknowledge research support from Spanish Ministry of Science and Technology through the research projects DPI2007-65601-C03-00, and the Spanish Ministry of Health through the research project FIS PI06-0446 and the Instituto Salud Carlos III (CIBER-BBN).

References

Alastrué, V., Peña, E., Martínez, M.A., Doblaré, M., 2008. Experimental study and constitutive modelling of the passive mechanical properties of the ovine infrarenal vena cava tissue. J. Biomech. 41, 3038–3045.
Alastrué, V., Rodríguez, J.F., Calvo, B., Doblaré, M., 2007. Structural damage models for fibrous biological soft tissues. Int. J. Solids Struct. 44, 5894–5911.
Balzani, D., Schröder, J., Gross, D., 2006. Simulation of discontinuous damage incorporating residual stress in circumferentially overstretched atherosclerotic arteries. Acta Biomater. 2, 609–618.
Bazant, Z.P., Jirasek, M., 2002. Nonlocal integral formulations of plasticity and damage: Survey of progress. J. Eng. Mech. 128, 1119–1149.
Calvo, B., Peña, E., Martínez, M.A., Doblaré, M., 2007. An uncoupled directional damage model for fibered biological soft tissues. Formulation and computational aspects. Int. J. Numer. Meth. Eng. 69, 2036–2057.
Dorfmann, A., Ogden, R.W., 2003. A pseudo-elastic model for loading, partial unloading and reloading of particle-reinforced rubber. Int. J. Solids Struct. 40, 2699–2714.
Dorfmann, A., Ogden, R.W., 2004. A constitutive model for the Mullins effect with permanent set in particle-reinforced rubber. Int. J. Solids Struct. 41, 1855–1878.
Ehret, A.E., Itskov, M., 2008. Modeling of anisotropic softening phenomena: Application to soft biological tissues. Int. J. Plasticity. doi:10.1016/j.ijplas.2008.06.001.
Flory, P.J., 1961. Thermodynamic relations for high elastic materials. Trans. Faraday Soc. 57, 829–838.
Franceschini, G., Bigoni, D., Regitnig, P., Holzapfel, G.A., 2006. Brain tissue deforms similarly to filled elastomers and follows consolidation theory. J. Mech. Phys. Solids 54, 2592–2620.
Fung, Y.C., 1993. Biomechanics. Mechanical Properties of Living Tissues. Springer-Verlag, New York.
Govindjee, S., Simo, J.C., 1992. Mullins' effect and the strain amplitude dependence of the storage modulus. Int. J. Solids Struct. 29, 1737–1751.
Hibbit, Karlsson, Sorensen, Inc., 2006. Abaqus user's guide, v. 6.5. HKS inc., Pawtucket, RI, USA.
Hokanson, J., Yazdami, S., 1997. A constitutive model of the artery with damage. Mech. Res. Commun. 24, 151–159.
Holzapfel, G.A., 2000. Nonlinear Solid Mechanics. Wiley, New York.
Holzapfel, G.A., 2001. Biomechanics of soft tissue. In: Lemaitre, J. (Ed.), Handbook of Materials Behavior Models, 3. Academic Press, New York, pp. 1057–1073.
Holzapfel, G.A., Gasser, C.T., Sommer, G., Regitnig, P., 2005. Determination of the layer-specific mechanical properties of human coronary arteries with non-atherosclerotic intimal thickening, and related constitutive modelling. Am. J. Physiol. Heart Circ. Physiol. 289, H2048–H2058.
Holzapfel, G.A., Gasser, T.C., Ogden, R.W., 2000. A new constitutive framework for arterial wall mechanics and a comparative study of material models. J. Elasticity 61, 1–48.
Humphrey, J.D., 2002. Continuum biomechanics of soft biological tissues. Proc. R. Soc. Lond. A 175, 1–44.
Hurschler, C., Loitz-Ramage, B., Vanderby, R., 1997. A structurally based stress–stretch relationship for tendon and ligament. ASMEJ Biomech. Eng. 119, 392–399.
Kaliske, M., Nasdala, L., Rothert, H., 2001. On damage modelling for elastic and viscoelastic materials at large strain. Comput. Struct. 79, 2133–2141.
Lanchares, E., Calvo, B., Cristóbal, J.A., Doblaré, M., 2008. Finite element simulation of arcuates for astigmatism correction. J. Biomech. 41, 797–805.
Liao, H., Belkoff, S.M., 1999. A failure model for ligaments. J. Biomech. 38, 183–188.
Marsden, J.E., Hughes, T.J.R., 1994. Mathematical Foundations of Elasticity. Dover, New York.
Martins, J., Pires, E., Salvado, R., Dinis, P., 1998. A numerical model of passive and active behavior of skeletal muscles. Comput. Methods Appl. Mech. Eng. 151, 419–433.
Miehe, C., 1995. Discontinuous and continuous damage evolution in Ogden-type large-strain elastic materials. Eur. J. Mech. A/Solids 14, 697–720.
Miehe, C., Keck, J., 2000. Superimposed finite elastic–viscoelastic–plastoelastic stress response with damage in filled rubbery polymers. Experiments, modelling and algorithmic implementation. J. Mech. Phys. Solids 48, 323–365.
Mullins, L., 1947. Effect of stretching on the properties of rubber. Rubber Res. 16, 275–289.
Mullins, L., Tobin, N., 1957. Theoretical model for the elastic behavior of filler-reinforced vulcanized rubbers. Rubber Chem. Tech. 30, 551–571.
Natali, A.N., Pavan, P.G., Carniel, E.L., Luisiano, M.E., Taglialavoro, G., 2005. Anisotropic elasto-damage constitutive model for the biomechanical analysis of tendons. Med. Eng. Phys. 27, 209–214.
Ogden, R.W., Roxburgh, D.G., 1999. A pseudo-elastic model for the Mullins effect in filled rubber. Proc. R. Soc. Lond. A A455, 2861–2878.
Peña, E., Calvo, B., Martínez, M.A., Doblaré, M., 2008a. On finite strain damage of viscoelastic fibered materials. Application to soft biological tissues. Int. J. Numer. Meth. Eng. 74, 1198–1218.
Peña, E., del Palomar, A.P., Calvo, B., Martínez, M.A., Doblaré, M., 2007. Computational modelling of diarthrodial joints. Physiological, pathological and pos-surgery simulations. Arch. Comput. Method Eng. 14 (1), 47–91.
Peña, E., Martínez, M.A., Calvo, B., Calvo, M.D., 2008b. Application of the natural element method to finite deformation inelastic problems in isotropic and fiber-reinforced biological soft tissues. Comput. Methods Appl. Mech. Eng. 197, 1983–1996.
Peña, E., Peña, J.A., Doblaré, M., 2008c. On modelling nonlinear viscoelastic effects in ligaments. J. Biomech. 41, 2659–2666.
Qi, H.J., Boyce, M.C., 2007. Constitutive model for stretch-induced softening of the stress–stretch behavior of elastomeric materials. J. Mech. Phys. Solids 52, 2187–2220.
Rodríguez, J.F., Alastrue, V., Doblaré, M., 2008. Finite element implementation of a stochastic three dimensional finite-strain damage model for fibrous soft tissue. Comput. Methods Appl. Mech. Eng. 197, 946–958.
Rodríguez, J.F., Cacho, F., Bea, J.A., Doblaré, M., 2006. A stochastic-structurally based three dimensional finite-strain damage model for fibrous soft tissue. J. Mech. Phys. Solids 54, 564–886.
Simo, J.C., 1987. On a fully three-dimensional finite-strain viscoelastic damage model: formulation and computational aspects. Comput. Methods Appl. Mech. Eng. 60, 153–173.

Simo, J.C., Ju, J.W., 1987. Strain- and stress-based continuum damage models. I. Formulation. Int. J. Solids Struct. 23, 821–840.
Souza-Neto, E.A., Peric, D., Owen, D.R.J., 1998. Continuum modelling and numerical simulation of material damage at finite strains. Arch. Comput. Method Eng. 5, 311–384.
Spencer, A.J.M., 1954. Theory of invariants. In: Continuum Physics. Academic Press, New York, pp. 239–253.
Volokh, K.Y., 2007a. Hyperelasticity with softening for modeling materials failure. J. Mech. Phys. Solids 55, 2237–2264.
Volokh, K.Y., 2007b. Prediction of arterial failure based on a microstructural bi-layer fiber–matrix model with softening. J. Biomech. 41, 447–453.
Weiss, J.A., Maker, B.N., Govindjee, S., 1996. Finite element implementation of incompressible, transversely isotropic hyperelasticity. Comput. Methods Appl. Mech. Eng. 135, 107–128.